

## In-Situ Modalities for Real-Time Melt Pool Characterization in Directed Energy Deposition Process Additive Manufacturing: A Review

Marcos Flores<sup>1,2</sup>, Ahmed Bendaouia<sup>2,3</sup>, Monsuru Ramoni and Jianzhi Li<sup>2,3</sup>

<sup>1</sup> Institute for Advanced Manufacturing (IAM), University of Texas Rio Grande Valley, United States.

<sup>2</sup> College of Engineering and Computer Science, University of Texas Rio Grande Valley

<sup>3</sup> Manufacturing and Industrial Engineering Department, University of Texas Rio Grande Valley, United States.

### **Abstract**

Build quality is one of the major factors hindering the wide adoption of additive manufacturing in many industries' productions, aerospace, and defense. In-situ monitoring is a fundamental step to achieve an overall improvement in printed parts. This review explores advanced optical monitoring and temperature measurement techniques used for in-situ monitoring laser-based additive manufacturing to understand melt pool dynamics during printing to improve build quality. High-speed imaging systems, calibrated illumination and optical filters, enable real-time visualization of melt pool dynamics. Techniques such as bandpass filtering, beam splitting, and synchronized laser illumination enhance signal clarity while protecting sensors. Deep learning approaches, including a real-time object detection algorithm "YOLO"; and convolutional neural networks, are increasingly used for automated detection of melt pool features and defects. In addition, pyrometers, ranging from single wavelength to multi-channel systems, provide non-contact temperature measurements across key thermal zones. These sensors are frequently calibrated using reference plates and thermocouples to ensure accuracy. Together, these monitoring methods support in-situ analysis and form the basis for developing closed-loop control systems. This paper provides a consolidated overview of current configurations, sensor capabilities, and trends, highlighting their critical role in the advancement of intelligent, high-performance additive manufacturing systems.

**Keywords:** In situ modalities, melt-pool data, melt-pool shape, Direct Energy Deposition (DED)

### **1. Introduction**

Directed energy deposition (DED) is one of the most common technologies for 3D printing metal alloys [1]. The metals AM market has grown in recent years much faster than either the polymers or ceramics segments. By 2027, the aerospace, automotive, and energy sectors may capture 52% of the total metals AM revenues. It is expected that AM-based repair will come up as an actual application along with new manufacturing technologies [2]. In this paper we present different sensors and mounting approaches for monitoring DED processes.

The rest of the paper is structured as follows: Section 2 presents the different types of sensors used in monitoring the DED process, Section 3 discuss mounting approaches to avoid obstruction. Section 4 present conclusions.

## 1.1 DED process

The ISO/ASTM 52900 defines the DED process as “process in which focused thermal energy is used to fuse materials by melting as they are being deposited” [3].

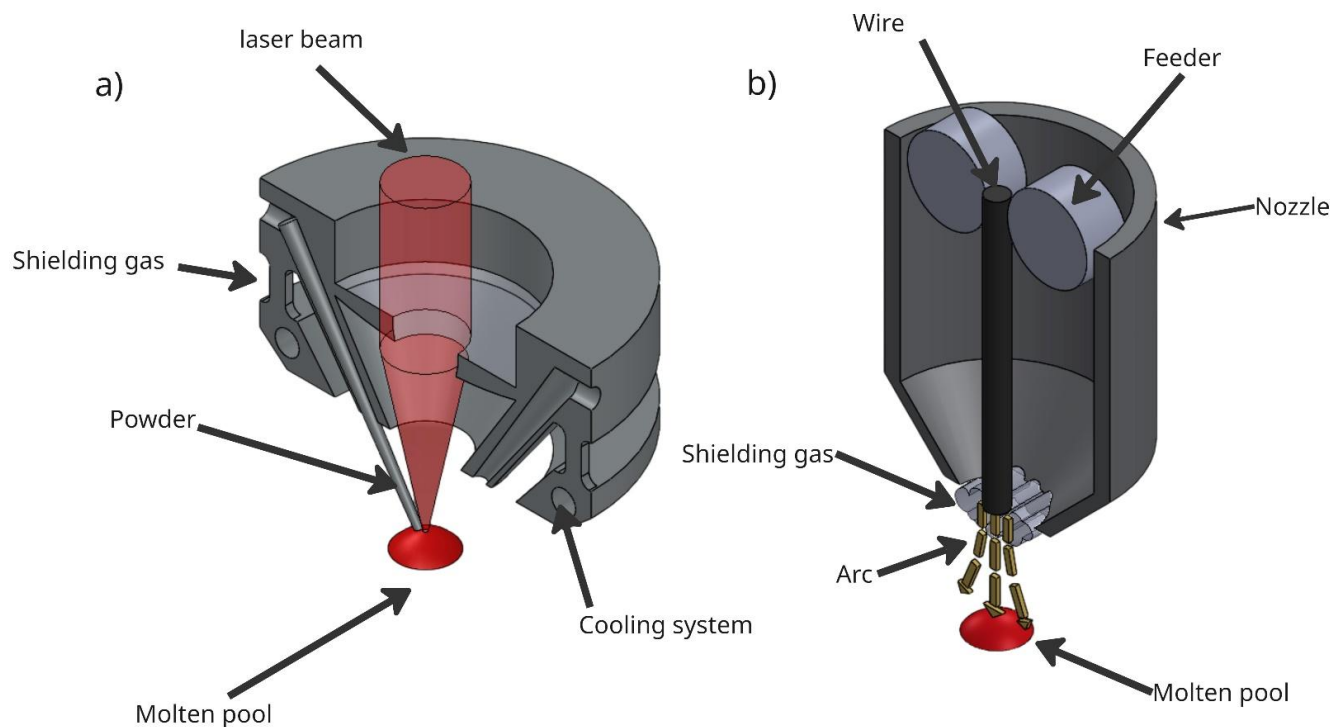
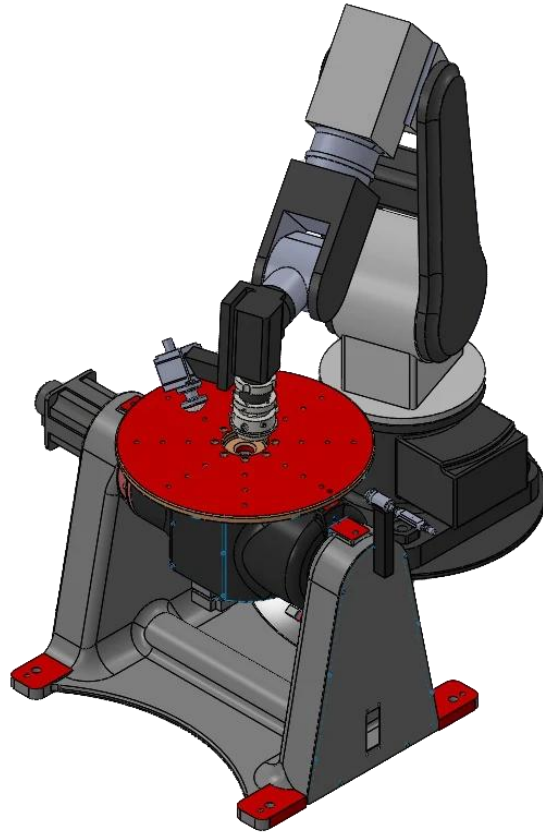


Figure 1 DED processes: a) Powder DED: the powder is injected with gas coaxially into the laser beam creating the melt pool. b) Wire DED: the material is fed in the form of a wire with a feeder and melted forming an electric arc.

DED is well-suited for the deposition of high-performance materials, including steels, titanium and aluminum alloys, ceramics, composites, and functionally graded materials (FGMs), offering lateral dimensional accuracy up to 0.05 mm [2][4]. The process creates a molten pool by melting both the feedstock and the underlying layer using focused thermal energy [5][6]. Powder-based systems apply cladding principles to repair components and introduce varied substrates within layers [7], while wire-based systems resemble welding and enable deposition outside enclosed environments using shielding gas [8]. Owing to its material versatility and efficiency, DED is widely used in aerospace, medical, and automotive applications to produce and repair metal components with reduced assembly requirements [1].

## 1.2 Process parameters

The DED process involves a series of complicated interactions among laser beam, powder and substrate under the inert gas shielding environment. Laser power, scan speed, beam size and powder flow rate are the dominant parameters that play a fundamental role in determining dimensional accuracy and metallurgical properties.[9]



*Figure 2 DED machine with a CMOS camera and 2-color pyrometer mounted*

The challenge of the DED process is that it is based on very complex dynamics and the potential involvement of more than one type of material, which can impact the quality and finish of the part if not properly monitored, the Laser-based DED process is sensible to the distance between the nozzle tip and surface, also the heat dissipation ability of the part is dependent on its geometry, and it can result in the local overheating on corners or thin walls.[10]

The size of the melt pool is one of the most important parameters in the process, ensuring constant melt pool size and geometry is fundamental to having uniform deposits of the substrates, hence, monitoring the size and shape of the melt pool is an important part of the quality control process.[11] Monitoring the thermal signatures of the process allows the prediction of microstructural evolution, mechanical properties and defect formation.[2]

## **2. Imaging and Thermal Monitoring of the DED process**

Multiple approaches have been used in terms of monitoring the melt pool:

### **2.1 CMOS cameras**

a)



b)



Figure 3 Complementary Metal Oxide Semiconductor cameras: a) Basler Ace1920 [12], b) Prosilica GT1930C[13]

The CMOS pixel sensors are exposed sequentially and convert the incident photons to a voltage which results in the pixel value.[14]. These cameras are used due to the lower cost, smaller pixels size and higher frame rates than most infrared cameras [15]

Type	Model	Connection	Resolution	Reference
CMOS camera	Basler, grayscale vision camera	Not Provided	1440 x 1080 pixels at 10fps	[16]
	Basler, Ace1920-160um	USB3.0	1920 x 1200 pixels at 160 fps	[17], [18]
	Prosilica GT1930C	Cat6, drag chain suitability 12 pin I/O port	1936 x 1216 pixels at 25 fps	[19]
	Ximea xiQ–USB3 MQ013xG-ON	USB3.0	1280 x 1024 at 61 fps	[15]
	Prosilica GC640	Cat6, drag chain suitability 12 pin I/O port	640 x 480 at 200 fps	[20]
	MER-301-125U3M	USB3.0	2048 x 1536 pixels at 125 fps	[21]
	Genie nano G3-GM10-M0800	Cat6 cable	-	[22]
	Balser acA1920-40gm	Cat6 6 pin I/O ports	1920 x 1216 pixels in 8 bits at 5 fps	[23]

Table 1 CMOS cameras used for monitoring the DED process

Monitoring melt pool shape enables effective tracking of heat accumulation, improving process stability, structural integrity, and productivity [16]. Lower accumulated heat reduces thermal stress and crack formation.

Camera-based methods have achieved high accuracy in melt pool width estimation, with deviations as low as 2.53% compared to microscopy [17]. Machine learning approaches, including CNNs, have been employed to analyze temperature and shape data, capturing temporal dynamics and melt pool fluctuations [18], [19].

Optical enhancements such as band-pass filters, dichroic mirrors, and image cropping help manage brightness and data size [15], [19]. Systems have incorporated complex optical paths—using mirrors, prisms, and notch filters—to protect sensors and improve signal quality [20], [21]. Dual-band imaging setups were simplified by splitting beams into a single camera using beam-splitting optics [21]. Image processing software has also been developed to extract features like melt pool area and coordinates from CMOS camera images [22], while NIR filtering techniques enhance detection by excluding the laser wavelength [23].

**2.2 CCD Cameras**



Figure 4 CM3-U3 monochrome camera [24]

In a CCD sensor, every pixel's charge is transferred through a very limited number of output nodes to be converted to voltage, buffered, and sent off chip as an analog signal. Concept design from [25]

Type	Model	Connection	Resolution	Reference
CCD camera	(CM3-U3-13Y3M, FLIR)	USB 3.0	1280 x 1024 pixels	[26]
	Not provided	-	-	[27]
	DMG MORI proprietary monitoring system	-	-	[28]
	Watec WAT-902B	RCA	768 x 494 pixels	[29]

Table 2 CCD cameras used in monitoring DED process

To enhance melt pool imaging and suppress interference from laser radiation and ambient light, various optical filtering and image processing techniques have been employed. A near-infrared (NIR) band-pass filter (840–865 nm) was used in [26] to block laser radiation (1080 nm) and visible light noise from metal powder scattering. Despite this, OpenCV-based preprocessing was necessary to further suppress residual noise and spatter artifacts for accurate region-of-interest (ROI) extraction.

Similarly, [27] uses a blocking filter centered at  $808 \pm 20$  nm to protect the CCD sensor from laser radiation. Image segmentation began with an adaptive triangle thresholding algorithm to detect areas of significant pixel change, followed by edge detection using the Canny method. The melt pool ROI was then cropped into a bounding rectangle, reducing both environmental noise and computational load for subsequent neural network processing.

In [28], a dichroic mirror directed melt pool radiation toward the camera, leveraging a spectral range with emissivity properties favorable for temperature analysis. Additionally, [29] employed a NIR band-pass filter (780–1000 nm) to isolate melt pool emissions while effectively eliminating reflections from the 1070 nm laser, ensuring clear imaging of the thermal process.

### 2.3 Weld and Thermal cameras

Digital, high dynamic range welding cameras, with this the operator can clearly observe the enlarged molten pool image remotely through a monitor, and the image can determine the position of the welding wire, the state of the welding pool. [30]

Type	Model	Connection	Resolution	Reference
Welding camera	monochrome XVC-1000	RJ45, Hirose Trigger connector	1280 x 1020 pixels	[31]
	Cavitar c300	RJ45, M12, X-coded	1440 x 1080 at 100 fps	[32]
	Cavitar	M12, X-coded	1440 x 1080 at 30 fps	[33]

Table 3 Welding cameras used in monitoring DED process

Type	Model	Connection	Resolution	Reference
Thermal camera	ThermaViz® TV200, Stratonics	Not provided	2048 x 1536 pixels at 1000 Fps 1000-2500C	[34]
	NIT TACHYON 1024	USB 2.0	32 x 32 pixels at 10 fps	[16]
	LumaSense MCS640	12 pin power connector, RJ45	640 x 480 pixels 600 to 3000C	[35]
	InfraTec Jade III MWIR	Not provided	320 x 240 pixels	[36]
	Pyroview 768N, DIAS Infrared Systems	Connector M23, M12A (Ethernet)	1000 – 3000C 768 x 576 pixels 25Hz	[37]
	X8500sc, FLIR Systems	GigE, USB, RS-232	1280 x 1024 pixels at 180 fps	[38]
	FLIR SC8300	GigE, USB, RS-232	256 x 180 pixels at 233hz	[39]

Table 4 Thermal cameras used in monitoring DED process

To address the high contrast between the intense laser-material interaction zone and its surroundings, [31] implemented a dimmable illumination source. A 75 mm lens combined with a 40 mm spacer enabled close-up visualization of the melt pool, while a UV filter was applied to suppress unwanted reflections within the region of interest.

YOLO (You Only Look Once), a widely used real-time object detection and instance segmentation algorithm, was introduced in [32]. This method utilizes a single convolutional neural network to concurrently predict object bounding boxes and class probabilities, offering fast and efficient image analysis capabilities suitable for monitoring dynamic processes.

In [33], image acquisition was performed at 30 frames per second (FPS) via Gigabit Ethernet (GigE) for storage and analysis. The Cavitar welding camera, designed specifically for high-intensity welding environments, featured 640 nm laser illumination and a proprietary filtering system to mitigate interference from the fusion process and laser radiation.

Various optical configurations and camera systems have been developed to optimize the monitoring of melt pool dynamics while minimizing interference from the additive manufacturing environment. In [34], The system maintained a working distance of  $245 \pm 30$  mm, with a fixed focal length of 42 mm, and incorporated a calibrated neutral density filter to prevent pixel saturation.

The system in [35] utilized a camera with a spectral sensitivity around 670 nm, allowing signal acquisition through the laser-blocking view glass of a Concept Laser machine. The camera was tripod-mounted close to the observation window for an unobstructed view of the process.

To enhance temperature measurement accuracy, [37] employed a near-infrared (NIR) camera operating in the 0.8–1.1  $\mu\text{m}$  range, minimizing the impact of emissivity variations. A laser-blocking filter centered at 1060 nm was added to protect the sensor from laser damage. Similarly, [38] utilized a beam splitter to direct melt pool radiation to an infrared camera, while a bandpass filter attenuated radiation intensity. This camera operated in the 3–5  $\mu\text{m}$  mid-wave infrared (MWIR) range, which is not affected by the printing laser wavelength (1.07  $\mu\text{m}$ ).

To detect cooler regions such as the melt pool tail, [39] selected an MWIR camera, as visible light cameras are limited to capturing emissions from high-temperature zones. MWIR imaging offers improved sensitivity to lower-temperature thermal features, enhancing the ability to characterize the full thermal profile of the melt pool.

## 2.5 High speed cameras

Type	Model	Connection	Resolution	Reference
High speed camera	Edgertronic SC2 +	10/100 Ethernet, 2 USB ports	1280 x 720 pixels at 2500 frames per second	[40]
	Fastcam Mini AX200, Photron	High-speed Gigabit Ethernet	1024 x 1024 pixels at 6000 fps	[41]
	Phantom miro 4	10/100 Ethernet	800 x 600 pixels up to 1260 fps	[42]
	Revealer, X213M	GigE Interface	1280 x 1024 pixels at 2000 fps	[43]
	Virtins Technology	-	832 x 496 pixels	[44]

Table 5 High speed cameras used in monitoring DED process

High-speed imaging systems have been widely adopted to observe melt pool behavior and transient dynamics during laser-based additive manufacturing processes.

To capture dynamic features while minimizing interference from process emissions, [41] employed a high-speed camera in conjunction with a synchronized external illumination system. A pulsed diode laser emitting at 640 nm was positioned laterally to illuminate the region of interest, approximately 30 mm in diameter. The reflected light was recorded by the high-speed camera, and a beam sizing lens coupled to a delivery fiber optimized illumination coverage.

Similarly, [42] used an off-axis camera installation supported by an external laser illumination source (Oxford Lasers Ltd). A bandpass filter (Edmund Optics) was mounted on the camera to suppress background light and isolate relevant image data. In [43], a CCD camera equipped with a narrowband optical filter was used to match the wavelength of the auxiliary lighting source, effectively enhancing visibility of the molten pool and potential defects by eliminating unrelated emissions.

**2.6 Pyrometers.**



Figure 5 a) Optris CTlaser 3M infrared thermometer [45], b) Sensortherm M3 series 2-color Pyrometer [46].

Type	Model	Connection	Resolution	Reference
Pyrometer	CT Video 2MH1CFV, Optris	USB	250C - 2200C	[26]
	Sensortherm, M332	RS232/RS485.	300 – 3000C	[17], [18]
	Optris CTlaser 3 M	USB, RS232, Profibus, Ethernet, Relay	50 – 400c	[19]
	Optris CT XL 3 M		200 – 1500c	
	Optris CTlaser 05 M		1000 – 2000c	
ThermaViz	-	752 x 480 pixels	[47]	

Table 6 Pyrometers used in monitoring of DED process

Pyrometers have been extensively utilized in additive manufacturing to measure melt pool temperatures with high temporal resolution and accuracy.

A two-color pyrometer capable of detecting infrared emissions in the 1400–1800 nm range was employed in [16], offering increased robustness to emissivity variations and surface conditions during the monitoring process.

To enable spatially distributed temperature measurements, [17] implemented a multi-pyrometer system consisting of three sensors with distinct operating ranges: 50–400 °C (Optris CTlaser 3M) for the leading edge, 200–1500 °C (Optris CT XL 3M) for the trailing edge, and 1000–2000 °C (Optris CTlaser 05M) for the melt pool. Each pyrometer was calibrated for emissivity using a heated reference plate and thermocouple-based contact measurements to ensure measurement accuracy across the different thermal zones.

### 3. Elemental analysis of DED melt pool



Figure 6 OCEANHDX-UV-VIS Spectrometer[48].

Optical Emission Spectroscopy (OES) is a valuable technique for real-time chemical analysis in laser-based additive manufacturing processes. OES operates by capturing the emission light from the plasma plume formed by vaporized metal species above the melt pool during laser-directed energy deposition (DED) [49]. By analyzing the spectral lines emitted from the process zone, OES enables the identification and comparison of elemental signatures from both the base material and the feedstock, offering insights into material composition throughout the build [50].

Type of sensor	Model	Connectivity	Range	Reference
UV-Vis Spectrometer	OCEANHDX-UV-VIS	Gigabit Ethernet, SMA 905 (input fiber), USB	200-800nm	[51]
UV-NIR spectrometer	Ocean Optics, Inc. HR4000 CG	USB, Serial ports	200 to 1100 nm	[52]

Optical process emissions in laser-based additive manufacturing can be effectively captured using ultraviolet-visible (UV-Vis) spectroscopy. In [45], process emissions were recorded with a UV-Vis spectrometer (OCEANHDX-UV-VIS, Ocean Insight, Orlando, FL, USA) operating over a spectral range of 200–800 nm. To

enhance visualization of the melt pool region, the area was illuminated with two auxiliary lasers emitting at  $810 \pm 10$  nm, providing consistent background lighting for accurate spectral acquisition.

In [46], a custom-designed sensor mounting fixture was developed to surround the laser processing head, enabling stable, close-range optical monitoring. A spectrometer fiber with a 400  $\mu\text{m}$  diameter silica core was integrated into the fixture and positioned 59.7 mm from the melt pool. The fiber's opening was protected by a UV-fused silica window to prevent contamination and damage during processing. This configuration allowed for efficient collection of optical emissions with minimal disruption to the laser-material interaction zone.

Real-time composition monitoring is particularly critical for controlling material integrity and minimizing elemental loss during rapid manufacturing processes. A fiber pig-tailed lens system has been utilized to collect plasma emissions at a fixed position relative to the substrate, efficiently directing the light to a high-resolution spectrometer. The system typically includes a 10- $\mu\text{m}$  entrance aperture, a holographic UV/VIS grating with 1200 grooves per millimeter, and a 2048-element CCD array, achieving a spectral resolution of 0.2 nm [53].

Additionally, advanced modeling approaches have been developed to enhance OES data interpretation. Physics-informed algorithms, supported by atomic emission spectrum simulations, have been applied to rapidly fit Laser-Induced Breakdown Spectroscopy (LIBS) data, accurately identifying emission peaks and predicting their locations and intensities, particularly for Fe and Ni species [49].

Overall, OES provides a powerful, non-contact method for real-time process monitoring, offering chemical composition tracking and potential pathways for closed-loop control in both DED and SLM systems.

#### **4. Mounting of Monitoring System For DED**

Various optical configurations have been implemented in Directed Energy Deposition (DED) to ensure accurate and unobstructed monitoring of the melt pool. In [33], a camera was mounted directly on the deposition head, maintaining a fixed focal distance of 200 mm and a  $50^\circ$  viewing angle relative to the horizontal plane. Similarly, an off-axis camera was positioned at a  $57^\circ$  angle in [34] to provide a clear, unobstructed view of the melt pool, avoiding interference from the laser head and deposition tool. In [36], the x-y scanner head was replaced with a thermal imaging system, which viewed the powder bed at a shallow  $5^\circ$  angle relative to the normal surface. This system employed a wide-angle lens with a 12 mm focal length, achieving an optical resolution of 1.5 mm per pixel.

High-speed imaging systems have also been utilized to capture rapid melt pool dynamics. In [40], a high-speed camera was mounted off-axis at a  $45^\circ$  inclination and mechanically coupled to the laser optics, ensuring a stable and focused image throughout the process. Similarly, in [44], a high-speed camera was installed at a  $50^\circ$  angle relative to the horizontal plane, with a working distance of 260 mm from the cladding surface, providing a consistent monitoring perspective.

In addition to visual monitoring, thermal measurements have been integrated into DED setups. In [26], a single-wavelength pyrometer was installed at a  $27^\circ$  angle and 170 mm from the melt pool, enabling real-time temperature acquisition to support process control and thermal analysis.

#### **4. Conclusion**

The integration of advanced sensing technologies in Directed Energy Deposition (DED) has significantly improved the ability to monitor, analyze, and control melt pool behavior and process dynamics in real time. Vision-based systems, such as CCD and CMOS cameras, enable precise tracking of melting pool dimensions and heat accumulation within the part, which are closely tied to the fluid dynamics and thermal behavior of the molten

material [16], [26]. Temperature, a critical factor influencing viscosity and droplet formation, can be effectively monitored using thermal cameras and pyrometric sensors [16], [17], [26]. The combined use of coaxially installed CMOS cameras and two-color pyrometers allows simultaneous acquisition of visual and thermal data across both visible and infrared spectra, improving the accuracy and reliability of melt pool monitoring [17], [18]. Additionally, comprehensive multi-sensor systems that collect visual, thermal, positional, chemical, and acoustic data offer a deeper understanding of the DED process [19]. These advanced monitoring strategies are essential for improving part quality, enabling real-time defect detection, and supporting the future development of closed-loop control systems in additive manufacturing.

### **Acknowledgement**

The authors would like to acknowledge funding provided by the U.S. Department of Energy NNSA MSIPP Program under Award No. DE-NA0004003. The opinions expressed in this paper are solely those of the authors, and do not necessarily represent those of the DOE/NNSA.

### **Declaration of Competing Interest**

The authors declare that they have no known competing financial interests or personal relationships that could have appeared to influence the work reported in this paper.

### **References**

- [1] M. Lalegani Dezaki *et al.*, “A review on additive/subtractive hybrid manufacturing of directed energy deposition (DED) process,” *Adv. Powder Mater.*, vol. 1, no. 4, p. 100054, Oct. 2022, doi: 10.1016/j.apmate.2022.100054.
- [2] D. Svetlizky *et al.*, “Directed energy deposition (DED) additive manufacturing: Physical characteristics, defects, challenges and applications,” *Mater. Today*, vol. 49, pp. 271–295, Oct. 2021, doi: 10.1016/j.mattod.2021.03.020.
- [3] “ISO/ASTM 52900(en), Additive manufacturing — General principles — Terminology.” Accessed: Feb. 19, 2025. [Online]. Available: <https://www.iso.org/obp/ui/#iso:std:iso-astm:52900:dis:ed-2:v1:en>
- [4] S. K. Everton, M. Hirsch, P. Stravroulakis, R. K. Leach, and A. T. Clare, “Review of in-situ process monitoring and in-situ metrology for metal additive manufacturing,” *Mater. Des.*, vol. 95, pp. 431–445, Apr. 2016, doi: 10.1016/j.matdes.2016.01.099.
- [5] D.-G. Ahn, “Directed Energy Deposition (DED) Process: State of the Art,” *Int. J. Precis. Eng. Manuf. - Green Technol.*, vol. 8, no. 2, pp. 703–742, Mar. 2021, doi: 10.1007/s40684-020-00302-7.
- [6] K. S. B. Ribeiro, F. E. Mariani, and R. T. Coelho, “A Study of Different Deposition Strategies in Direct Energy Deposition (DED) Processes,” *Procedia Manuf.*, vol. 48, pp. 663–670, Jan. 2020, doi: 10.1016/j.promfg.2020.05.158.
- [7] “Component repair using laser direct metal deposition,” ResearchGate. Accessed: Feb. 19, 2025. [Online]. Available: [https://www.researchgate.net/publication/228895143\\_Component\\_repair\\_using\\_laser\\_direct\\_metal\\_deposition](https://www.researchgate.net/publication/228895143_Component_repair_using_laser_direct_metal_deposition)
- [8] W. J. Sames, F. A. List, S. Pannala, R. R. Dehoff, and S. S. Babu, “The metallurgy and processing science of metal additive manufacturing,” *Int. Mater. Rev.*, vol. 61, no. 5, pp. 315–360, Jul. 2016, doi: 10.1080/09506608.2015.1116649.
- [9] L. Song, V. Bagavath-Singh, B. Dutta, and J. Mazumder, “Control of melt pool temperature and deposition height during direct metal deposition process,” *Int. J. Adv. Manuf. Technol.*, vol. 58, no. 1, pp. 247–256, Jan. 2012, doi: 10.1007/s00170-011-3395-2.
- [10] A. Urresti, O. Murua, J. I. Arrizubieta, and A. Lamikiz, “In-situ monitoring of the DED-LB process for defect detection,” *Procedia CIRP*, vol. 124, pp. 314–317, Jan. 2024, doi: 10.1016/j.procir.2024.08.125.

- [11] S. Barua, F. Liou, J. Newkirk, and T. Sparks, "Vision-based defect detection in laser metal deposition process," *Rapid Prototyp. J.*, vol. 20, no. 1, pp. 77–85, Jan. 2014, doi: 10.1108/RPJ-04-2012-0036.
- [12] "ace 2 a2A1920-160umPRO | USB 3.0 Camera | Basler | Basler AG." Accessed: Jul. 07, 2025. [Online]. Available: <https://www.baslerweb.com/en-us/shop/a2a1920-160umpro/>
- [13] "Detail," Allied Vision. Accessed: Jul. 07, 2025. [Online]. Available: <https://www.alliedvision.com/en/camera-selector/detail/>
- [14] C. Danakis, M. Afgani, G. Povey, I. Underwood, and H. Haas, "Using a CMOS camera sensor for visible light communication," in *2012 IEEE Globecom Workshops*, Dec. 2012, pp. 1244–1248. doi: 10.1109/GLOCOMW.2012.6477759.
- [15] L. Mazzoleni, A. G. Demir, L. Caprio, M. Pacher, and B. Previtali, "Real-Time Observation of Melt Pool in Selective Laser Melting: Spatial, Temporal, and Wavelength Resolution Criteria," *IEEE Trans. Instrum. Meas.*, vol. 69, no. 4, pp. 1179–1190, Apr. 2020, doi: 10.1109/TIM.2019.2912236.
- [16] P. Stavropoulos, G. Pastras, K. Tzimanis, and N. Bourlesas, "Addressing the challenge of process stability control in wire DED-LB/M process," *CIRP Ann.*, vol. 73, no. 1, pp. 129–132, Jan. 2024, doi: 10.1016/j.cirp.2024.04.021.
- [17] S. H. Ji, "Investigation of melt pool monitoring-based deposition quality prediction in directed energy deposition".
- [18] S. H. Ji, T. H. Ko, J. Yoon, S. H. Lee, and H. Lee, "Coaxial melt pool monitoring with pyrometer and camera for hybrid CNN-based bead geometry prediction in directed energy deposition," *Precis. Eng.*, vol. 94, pp. 1–12, Jun. 2025, doi: 10.1016/j.precisioneng.2025.02.016.
- [19] N. D. Jamnikar, S. Liu, C. Brice, and X. Zhang, "In-process comprehensive prediction of bead geometry for laser wire-feed DED system using molten pool sensing data and multi-modality CNN," *Int. J. Adv. Manuf. Technol.*, vol. 121, no. 1, pp. 903–917, Jul. 2022, doi: 10.1007/s00170-022-09248-3.
- [20] M. Akbari and R. Kovacevic, "An investigation on mechanical and microstructural properties of 316LSi parts fabricated by a robotized laser/wire direct metal deposition system," *Addit. Manuf.*, vol. 23, pp. 487–497, Oct. 2018, doi: 10.1016/j.addma.2018.08.031.
- [21] C. Hao, Z. Liu, H. Xie, K. Zhao, and S. Liu, "Real-time measurement method of melt pool temperature in the directed energy deposition process," *Appl. Therm. Eng.*, vol. 177, p. 115475, Aug. 2020, doi: 10.1016/j.applthermaleng.2020.115475.
- [22] K. S. B. Ribeiro, H. H. L. Núñez, J. B. Jones, P. Coates, and R. T. Coelho, "A novel melt pool mapping technique towards the online monitoring of Directed Energy Deposition operations," *Procedia Manuf.*, vol. 53, pp. 576–584, Jan. 2021, doi: 10.1016/j.promfg.2021.06.058.
- [23] A. Da Silva, J. Frostevarg, and A. F. H. Kaplan, "Melt pool monitoring and process optimisation of directed energy deposition via coaxial thermal imaging," *J. Manuf. Process.*, vol. 107, pp. 126–133, Dec. 2023, doi: 10.1016/j.jmapro.2023.10.021.
- [24] "Teledyne Imaging FLIR/IIS Chameleon®3 | Edmund Optics." Accessed: Jul. 07, 2025. [Online]. Available: <https://www.edmundoptics.com/f/flir-chameleon3-usb-30-cameras/15023/>
- [25] "CCD and CMOS Technology." Accessed: Apr. 24, 2025. [Online]. Available: [https://www.tedpella.com/cameras\\_html/ccd\\_cmos.aspx](https://www.tedpella.com/cameras_html/ccd_cmos.aspx)
- [26] H. Shin, J. Lee, S.-K. Choi, and S. W. Lee, "Development of multi-defect diagnosis algorithm for the directed energy deposition (DED) process with in situ melt-pool monitoring," *Int. J. Adv. Manuf. Technol.*, vol. 125, no. 1, pp. 357–368, Mar. 2023, doi: 10.1007/s00170-022-10711-4.
- [27] J. Yuan, H. Liu, W. Liu, F. Wang, and S. Peng, "A method for melt pool state monitoring in laser-based direct energy deposition based on DenseNet," *Measurement*, vol. 195, p. 111146, May 2022, doi: 10.1016/j.measurement.2022.111146.
- [28] C. Kledwig, H. Perfahl, M. Reisacher, F. Brückner, J. Bliedtner, and C. Leyens, "Analysis of Melt Pool Characteristics and Process Parameters Using a Coaxial Monitoring System during Directed Energy

- Deposition in Additive Manufacturing,” *Materials*, vol. 12, no. 2, Art. no. 2, Jan. 2019, doi: 10.3390/ma12020308.
- [29] L. Chen, X. Yao, Y. Chew, F. Weng, S. K. Moon, and G. Bi, “Data-Driven Adaptive Control for Laser-Based Additive Manufacturing with Automatic Controller Tuning,” *Appl. Sci.*, vol. 10, no. 22, Art. no. 22, Jan. 2020, doi: 10.3390/app10227967.
- [30] ChuangPeng, “Seam Tracking System and Weld Pool Monitoring camera | Weld Navigator Laser Displacement Sensor,” Seam Tracking System and Weld Pool Monitoring camera | Weld Navigator Laser Displacement Sensor. Accessed: Apr. 25, 2025. [Online]. Available: [https://www.atiny-lasersensor.com/products/welding-monitoring-camera.html?gad\\_source=1&gbraid=0AAAAAojKQztwprwMyFeP\\_r8vWVm7EtfSz&gclid=Cj0KCQjw5azABhD1ARIsAA0WFUEJ3oV-x-YR2AvLHEKom5lu5G4RfAksPbb0sJ3r4besEVDmwEVrIk0aAqLSEALw\\_wcB](https://www.atiny-lasersensor.com/products/welding-monitoring-camera.html?gad_source=1&gbraid=0AAAAAojKQztwprwMyFeP_r8vWVm7EtfSz&gclid=Cj0KCQjw5azABhD1ARIsAA0WFUEJ3oV-x-YR2AvLHEKom5lu5G4RfAksPbb0sJ3r4besEVDmwEVrIk0aAqLSEALw_wcB)
- [31] D. S. Ertay, M. A. Naiel, M. Vlasea, and P. Fieguth, “Process performance evaluation and classification via in-situ melt pool monitoring in directed energy deposition,” *CIRP J. Manuf. Sci. Technol.*, vol. 35, pp. 298–314, Nov. 2021, doi: 10.1016/j.cirpj.2021.06.015.
- [32] R. Asadi *et al.*, “Process monitoring by deep neural networks in directed energy deposition: CNN-based detection, segmentation, and statistical analysis of melt pools,” *Robot. Comput.-Integr. Manuf.*, vol. 87, p. 102710, Jun. 2024, doi: 10.1016/j.rcim.2023.102710.
- [33] J. Flores, I. Cabanes, A. Gutierrez, K. L. de Calle, O. Gonzalo, and E. Portillo, “An innovative smart monitoring system for DED-LB/MW process stability based on machine learning techniques,” *Int. J. Adv. Manuf. Technol.*, vol. 137, no. 3, pp. 1759–1773, Mar. 2025, doi: 10.1007/s00170-025-15134-5.
- [34] I. Z. Era *et al.*, “In-Situ Melt Pool Characterization via Thermal Imaging for Defect Detection in Directed Energy Deposition Using Vision Transformers,” Feb. 11, 2025, *arXiv*: arXiv:2411.12028. doi: 10.48550/arXiv.2411.12028.
- [35] B. Cheng, J. Lydon, K. Cooper, V. Cole, P. Northrop, and K. Chou, “Melt pool sensing and size analysis in laser powder-bed metal additive manufacturing,” *J. Manuf. Process.*, vol. 32, pp. 744–753, Apr. 2018, doi: 10.1016/j.jmapro.2018.04.002.
- [36] A. Wegner and G. Witt, “PROCESS MONITORING IN LASER SINTERING USING THERMAL IMAGING”.
- [37] Z. Zhang, Z. Liu, and D. Wu, “Prediction of melt pool temperature in directed energy deposition using machine learning,” *Addit. Manuf.*, vol. 37, p. 101692, Jan. 2021, doi: 10.1016/j.addma.2020.101692.
- [38] I. Jeon, P. Liu, and H. Sohn, “Real-time melt pool depth estimation and control during metal-directed energy deposition for porosity reduction,” *Int. J. Adv. Manuf. Technol.*, Jun. 2023, doi: 10.1007/s00170-023-11689-3.
- [39] M. A. Hassan, M. Hassan, C.-G. Lee, and A. Sadek, “Monitoring Variability in Melt Pool Spatiotemporal Dynamics (VIMPS): Towards Proactive Humping Detection in Additive Manufacturing,” *J. Manuf. Mater. Process.*, vol. 8, no. 3, Art. no. 3, Jun. 2024, doi: 10.3390/jmmp8030114.
- [40] A. Assad *et al.*, “Process mapping and anomaly detection in laser wire directed energy deposition additive manufacturing using in-situ imaging and process-aware machine learning,” *Mater. Des.*, vol. 245, p. 113281, Sep. 2024, doi: 10.1016/j.matdes.2024.113281.
- [41] M. Motta, A. G. Demir, and B. Previtali, “High-speed imaging and process characterization of coaxial laser metal wire deposition,” *Addit. Manuf.*, vol. 22, pp. 497–507, Aug. 2018, doi: 10.1016/j.addma.2018.05.043.
- [42] Z. Sun, W. Guo, and L. Li, “In-process measurement of melt pool cross-sectional geometry and grain orientation in a laser directed energy deposition additive manufacturing process,” *Opt. Laser Technol.*, vol. 129, p. 106280, Sep. 2020, doi: 10.1016/j.optlastec.2020.106280.

- [43] J. Yang *et al.*, “High-Precision and Ultraspeed Monitoring of Melt-Pool Morphology in Laser-Directed Energy Deposition Using Deep Learning,” *Addit. Manuf. Front.*, p. 200199, Feb. 2025, doi: 10.1016/j.amf.2025.200199.
- [44] Z. Yang *et al.*, “In-situ monitoring of the melt pool dynamics in ultrasound-assisted metal 3D printing using machine learning,” *Virtual Phys. Prototyp.*, vol. 18, no. 1, p. e2251453, Dec. 2023, doi: 10.1080/17452759.2023.2251453.
- [45] “Optris CTlaser 3M Infrared Thermometer For Low Metal Temps,” United States. Accessed: Jul. 07, 2025. [Online]. Available: <https://optris.com/us/products/infrared-thermometers-pyrometers/ctlaser-series/ctlaser-3m/>
- [46] “METIS M322 (2-Color Pyrometer),” Sensortherm. Accessed: Jul. 07, 2025. [Online]. Available: <https://www.sensortherm.de/en/product/metis-m322-2-color-pyrometer/>
- [47] Z. Smoqi *et al.*, “Closed-loop control of meltpool temperature in directed energy deposition,” *Mater. Des.*, vol. 215, p. 110508, Mar. 2022, doi: 10.1016/j.matdes.2022.110508.
- [48] “Ocean HDX Spectrometer | Ocean Optics.” Accessed: Jul. 07, 2025. [Online]. Available: <https://www.oceanoptics.com/spectrometer/ocean-hdx/>
- [49] B. Squires *et al.*, “Laser-Induced Breakdown Spectroscopy for composition monitoring during directed energy deposition of graded Fe-Ni alloys,” *Int. J. Adv. Manuf. Technol.*, vol. 132, no. 7, pp. 3877–3888, Jun. 2024, doi: 10.1007/s00170-024-13578-9.
- [50] M. Schmidt, K. Partes, R. Rajput, G. Phochkhua, and H. Köhler, “Monitoring the degree of dilution during directed energy deposition of aluminum bronze and H13 tool steel using optical emission spectroscopy,” *J. Laser Appl.*, vol. 35, no. 4, p. 042058, Nov. 2023, doi: 10.2351/7.0001081.
- [51] M. Schmidt, H. Naesstroem, J. Volpp, and K. Partes, “Relating melt mixing, dilution and vapor emissions during directed energy deposition,” *Opt. Laser Technol.*, vol. 181, p. 111824, Feb. 2025, doi: 10.1016/j.optlastec.2024.111824.
- [52] A. R. Nassar, T. J. Spurgeon, and E. W. Reutzel, “Sensing Defects during Directed-Energy Additive Manufacturing of Metal Parts using Optical Emissions Spectroscopy,” 2014, Accessed: Jul. 02, 2025. [Online]. Available: <https://hdl.handle.net/2152/88750>
- [53] L. Song and J. Mazumder, “Real Time Cr Measurement Using Optical Emission Spectroscopy During Direct Metal Deposition Process,” *IEEE Sens. J.*, vol. 12, no. 5, pp. 958–964, May 2012, doi: 10.1109/JSEN.2011.2162316.